Heterostructures of ZnO Nanorods with Various One-Dimensional Nanostructures

Seung Yong Bae,[†] Hee Won Seo,[†] Hyun Chul Choi,[†] Jeunghee Park,*[,†] and Jucheol Park[‡]

Department of Chemistry, Korea University, Jochiwon 339-700, Republic of Korea, and Samsung Advanced Institute of Technololgy, Suwon 440-600, Republic of Korea

Received: March 10, 2004; In Final Form: June 10, 2004

High-density ZnO nanorods can be grown on pregrown one-dimensional nanostructures via thermal chemical vapor deposition of Zn at a low temperature of 500 °C, producing various heterostructures. We demonstrate it using carbon nanotubes, GaN nanowires, GaP nanowires, SiC nanowires, and SiC core−C shell coaxial nanocables. The diameter of ZnO nanorods is in the range of 80−150 nm, and the maximum length is about 3 μm. The ZnO nanorods align vertically on the walls of 1D nanostructures, with a uniform growth direction of [001]. We suggest a vapor−liquid−solid growth mechanism that Zn vapor deposits on the 1D nanostructures and produces the outer layers encapsulating the 1D nanostructures; the ZnO nanorods are grown out from the outer layers of the nanocable structure. The length and density of ZnO nanorods are controllable by the deposition time. All of these heterostructures exhibit intense UV photoluminescence and cathodoluminescence. The green emission intensity is correlated with the density of the ZnO nanorods.

1. Introduction

Since the discovery of carbon nanotubes (CNTs), current research is driving toward the nanoscale phenomena and technology.[1] The one-dimensional (1D) semiconductor nanostructures have attracted considerable research activities because of their great potential for fundamental studies of the role of dimensionality and size in the physical properties as well as for applications in electronic and optoelectronic nanodevices.[2] The formation of heterostructures is believed to be of importance in tailoring the physical properties of 1D nanostructures.[3−6] The heterostructures with various compositions and interfaces have already demonstrated the distinctive performance in naonodevice applications.[5b]

Zinc oxide (ZnO), a semiconductor with a direct wide band gap (3.37 eV at room temperature) and large exciton binding energy (60 meV), is one of the most promising materials for the fabrication of optoelectronic devices operating in the blue and ultraviolet (UV) region and for gas sensing applications.[7,8] The synthesis, characterization, and application of various 1D ZnO nanostructures including the rods/wires,[9] tubes,[10] belts/ribbons,[11] tetrapods,[12] needles/pins,[13,14] columns,[15] combs,[16] sheets,[17] and complex structures[18] are presently the subject of intense research. Moreover, the ZnO heterostructures have been synthesized for nanocables with $Zn(OH)_2$, ZnS, Ga, Al_2O_3, SiO_2, and Zn;[10a,b,h,19] nanorods on CNTs and In_2O_3 nanowires;[20] and heterojunction of MgO and Ni.[21] However, the development of new heterostructures still remains a challenging subject.

In this paper, we report a large-scale synthesis of various ZnO heterostructures and detailed evaluation of their structural and optical properties. The ZnO nanorods were grown on diverse pregrown 1D nanostructures via thermal chemical vapor deposition (CVD) of Zn at a low temperature of 500 °C. The pregrown 1D nanostructures are vertically aligned CNTs, partially vertical-aligned GaN nanowires, GaP nanowires, SiC nanowires, and SiC core−C shell coaxial nanocables whose syntheses have already been reported.[22−26] The use of Ga or In as a catalyst leads to the high yield of ZnO nanorods. The size and morphology of the nanostructures were thoroughly examined using electron microscopy, X-ray diffraction, and Raman spectroscopy. We then characterized the optical properties of these ZnO heterostructures by photoluminescence and cathodoluminescence.

2. Experimental Section

The syntheses of the CNTs, GaN nanowires, GaP nanowires, SiC nanowires, and SiC core−C shell coaxial nanocables have been described elsewhere.[22−26] The vertically aligned CNTs were grown on Fe nanoparticles-deposited silicon (Si) substrates using thermal CVD of C_2H_2.[22] The GaN nanowires were grown on Au nanoparticles-deposited Si substrates using CVD of a Ga/GaN mixture under NH_3 flow.[23] Part of them align vertically on the substrates. The GaP nanowires were grown randomly on Ni nanoparticles-deposited Si substrates via a sublimation of ball-milled GaP powders.[24] The aligned SiC nanowires and SiC−C nanocables were grown on Fe nanoparticles-deposited Si substrates using CVD of CH_4.[25,26] The Ga/GaN mixture was used as a cocatalyst. The synthesis method and the morphology are summarized in Table 1. All have a cylindrical shape, except the GaN nanowires have a unique triangle cross-section. The density of 1D nanostructures is in the range 10^9−10^{11} cm^{-2}. The vertically aligned CNTs have the highest density.

Zn (99.998%, Aldrich) powders mixed with Ga (99.999%, Aldrich) or In (99.999%, Aldrich) were placed in a quartz boat located inside a quartz tube reactor of electrical furnace. The CNTs (or GaN, GaP, SiC, SiC−C nanostructures)-grown substrates were placed on the boat containing Zn/Ga (or In). The temperature of the reactor was maintained at 500 °C. The growth time is in the range from 30 min to 4 h. Argon flowed constantly with a rate of 500 standard cubic centimeters per minute (sccm). The residual oxygen was incorporated into the growth of ZnO nanowires. The as-grown materials on the

* Corresponding author. E-mail: parkjh@korea.ac.kr.
[†] Korea University.
[‡] Samsung Advanced Institute of Technology.

10.1021/jp048918q CCC: $27.50
Published on Web 07/23/2004

TABLE 1: Summary of the Synthesis Method and the Morphology of Various ZnO Heterostructures Grown for 2 h

	pregrown 1D nanostructures					ZnO nanorods		heterostructures	
	synthesis methods (catalysts)	average diameter (nm)	length (μm)	density and alignment on the substrates	ref	average diameter (nm)	length (μm)	diameter (μm)	relative density of ZnO nanorods
CNTs	CVD of acetylene at 900 °C (Fe nanoparticles)	50 (30−100)[a]	~30	$>10^{10}$ cm^{-2} (highest), vertically aligned on Si substrates	22	80	0.3	0.5	middle
GaN nanowires	CVD of Ga/GaN under NH_3 flow at 900−1000 °C (Au nanoparticles)	50 (triangle cross-section)[b]	~30	~10^9 cm^{-2}, partially vertical-a ligned on alumina substrates	23	100	1.5	3	low
GaP nanowires	sublimati on of ball-milled GaP powders at 1000−1100 °C (Ni nanoparticles)	50	~500	~10^9 cm^{-2}, randomly on alumina substrates	24	150	0.7	1.5	low
SiC nanowires	Ga/GaN-assisted CVD of the Si substrates and CH_4 at 1100 °C (Fe nanoparticles)	50	~300	10^9−10^{10} cm^{-2}, randomly on Si substrates	25	100	0.5	1	middle
SiC−C coaxial nanocables	CVD of CH_4 following the growth of SiC nanowires at 1000 °C (Fe nanoparticles)	40[c] (SiC core: 20)	~300	10^9−10^{10} cm^{-2}, randomly on Si substrates	26	150	3	5	high

[a] CNTs have a broader diameter range than the others. [b] GaN nanowires have a triangle cross-section, while the others are cylindrical. [c] The diameter of the SiC core is 20 nm, and that of graphite layers is 10 nm.

substrate were characterized and analyzed by scanning electron microscopy (SEM, Hitachi S-4300), high-resolution transmission electron microscopy (TEM, JEOL JEM-2010, 200 kV), energy-dispersive X-ray spectroscopy (EDX), electron diffraction (ED), powder X-ray diffraction (XRD, Philips X'PERT MPD), and Raman spectroscopy (Renishaw) using 514.5 nm argon ion laser. Photoluminescence (PL) was conducted at room temperature (300 K) with the 325 nm line of a helium−cadmium (He−Cd) laser. The laser power was about 1 kW/ cm^2. The room-temperature cathodoluminescence (CL, Gatan MonoCL2) measurement was performed using an acceleration voltage of 10 kV.

3. Results and Discussion

(1) Morphology of the ZnO Nanorods Grown on 1D Nanostructures. White products were deposited on the whole substrates for 2 h. The SEM image reveals that the products are homogeneously the ZnO heterostructures. Figure 1a corresponds to a view showing that the ZnO nanorods decorate the vertically aligned CNTs grown on the Si substrate. A top view shows that high-density ZnO nanorods cover up the tip part of CNTs (Figure 1b). A magnified image reveals that the ZnO nanorods surround randomly the surface of CNTs (Figure 1c). Yet the diameter and length of ZnO nanorods are uniformly 80 and 300 nm, respectively. Further analyses described below confirm that the CNT exists as a core of these nanostructures. We observed that the growth of ZnO nanorods takes place from the tip part of CNTs to the bottom part.

Figure 1d shows a top view for the ZnO nanorods grown on the vertically aligned GaN nanowires. A magnified SEM image reveals a coniferous forest-like morphology of the nanostructures (Figure 1e). The majority of the nanorods align to the core axis with 3-fold symmetries, although some of them grow randomly (Figure 1f). The average diameter and length of the ZnO nanorods are 100 nm and 1.5 μm, respectively. Figure 1g corresponds to the ZnO nanorods grown on the GaP nanowires. A magnified image reveals a forsythia-like morphology of the nanostructures (Figure 1h). The bare GaP nanowires without any deposited ZnO nanorods still remain after 2 h deposition. The ZnO nanorods are grown with random direction on the surface of GaP nanowires. The diameter of ZnO nanorods is 150 nm, and the length is 0.7 μm.

Figure 1i corresponds to a top view of SiC nanowire/ZnO nanorod heterostructures grown on the substrate. The SiC nanowires have an average length of 300 μm and are ornamented with the ZnO nanorods having a diameter of 100 nm and a length of 0.5 μm. The diameter of the heterostructures is about 1 μm. Figure 1j shows a top view of the nanostructures of SiC−C coaxial nanocables deposited with a much higher-density ZnO nanorod as compared to the others. It reveals a foxtail-like morphology of the nanostructures that the diameter reaches to 5 μm (Figure 1k). The diameter and length of the ZnO nanorods are uniformly 150 nm and 3 μm, respectively (Figure 1l).

The morphology of the deposited ZnO nanorods and their heterostructures with five different 1D nanostructures are summarized in Table 1. The diameter of ZnO nanorods is in the range 80−150 nm. The 3-fold symmetric alignment of ZnO nanorods was observed only for the GaN nanowires whose cross-section is triangle. For a given growth time of 2 h, the length, diameter, and density are dependent on the 1D nanostructures. We observed that the length and density of ZnO nanorods can increase with the deposition time. The diameter is either uniform or increased with time. Among the five heterostructures grown for 2 h, the length and density of ZnO nanorods are largest for SiC−C coaxial nanocables. The lowest-density ZnO nanorods deposit on the GaN and GaP nanowires. The length of the ZnO nanorods is shortest in the case of CNTs, so the diameter of the heterostructures is only 500 nm. We will discuss these results in section 3 (Growth Mechanism of ZnO Nanorods).

(2) Structure and Composition Analysis: TEM, ED, EDX, XRD, and Raman Spectroscopy. The TEM image of GaN−ZnO nanostructures reveals that the ZnO nanorod array grows vertically on the wall of the GaN nanowire (Figure 2a). The average diameter of ZnO nanorods is 100 nm. The selected-area ED (SAED) pattern shows that the single-crystalline wurtzite ZnO nanorods are uniformly grown with the [001] growth direction. Because the GaN nanowire has the [100] growth direction, the ED pattern of ZnO and GaN crystals is

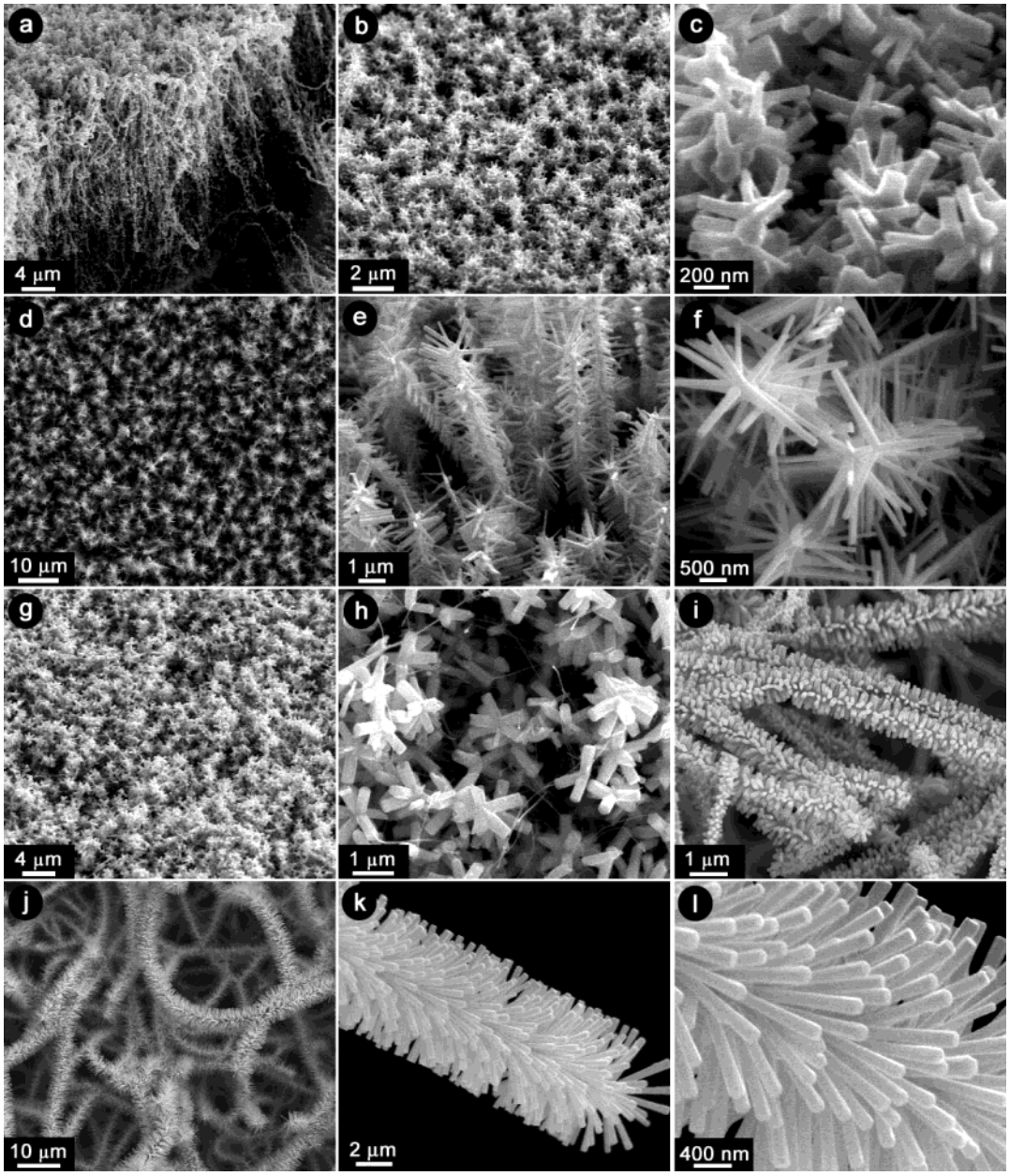

Figure 1. SEM micrographs of ZnO nanorods grown on (a−c) CNTs, (d−f) GaN nanowires, (g, h) GaP nanowires, (i) SiC nanowires, and (j−l) SiC−C nanocables.

overlapped as shown in the inset. Figure 2b shows the atomic-resolved image for a selected area of the ZnO nanorod marked by the arrow in Figure 2a. The [001] direction of the hexagonal unit cell is parallel to the long axis of the ZnO nanorod. The (001) fringes are separated by 5.2 Å, which is consistent with that of the bulk wurtzite ZnO crystal (a = 3.24982 Å, c = 5.20661 Å; JCPDS Card No. 36-1451). No stacking faults are found in the lattice planes, showing a nearly perfect ZnO crystal. Figure 2c shows EDX data, revealing clearly the existence of the Ga component for the core region (marked by the arrow "A" in Figure 2a), while only Zn and O components exist for the side region (marked by the arrow "B" in Figure 2a). Figure 2d displays the EDX line-scan profile of Zn, Ga, O, and N elements for a GaN−ZnO nanostructure whose TEM image is shown in the inset. It confirms the Ga component at the core region and Zn component at the outerlayers.

The XRD pattern obtained from the CNT−ZnO and GaN−ZnO heterostructures is displayed in Figure 3. The XRD peaks of the CNT−ZnO nanostructures are indexed to the wurtzite structured ZnO crystal (Figure 3a). The relative peak intensity is nearly the same as that of the powder. The XRD peaks from the CNTs were not detected due to the covered ZnO nanorods. Figure 3b corresponds to the XRD pattern obtained from the GaN−ZnO nanostructures. The peaks are indexed to the wurtzite structure GaN and ZnO crystals. The position of each GaN peak is consistent with that of the GaN bulk (JCPDS Card No. 76-0703).[24] The GaN peaks originate from the GaN nanowire cores that are not covered with the ZnO nanorods. No other crystalline forms are detected. Notice that the (002) peak of ZnO is much weaker than the (100) and (101) peaks. The intensity of the (002) peak is one-fifth that of the (101) peak, which is different from the XRD pattern of the CNT−ZnO nanostructures where the intensity of the (002) peaks is about one-half that of (101) peak. For the present vertically aligned GaN−ZnO nanostructures, the (001) planes of the ZnO nanorods are perpendicular to the substrate. The XRD cannot reflect much the lattice planes perpendicular to the substrates, which rationalize the diminished intensity of the (002) peaks. Therefore, the relative intensity of

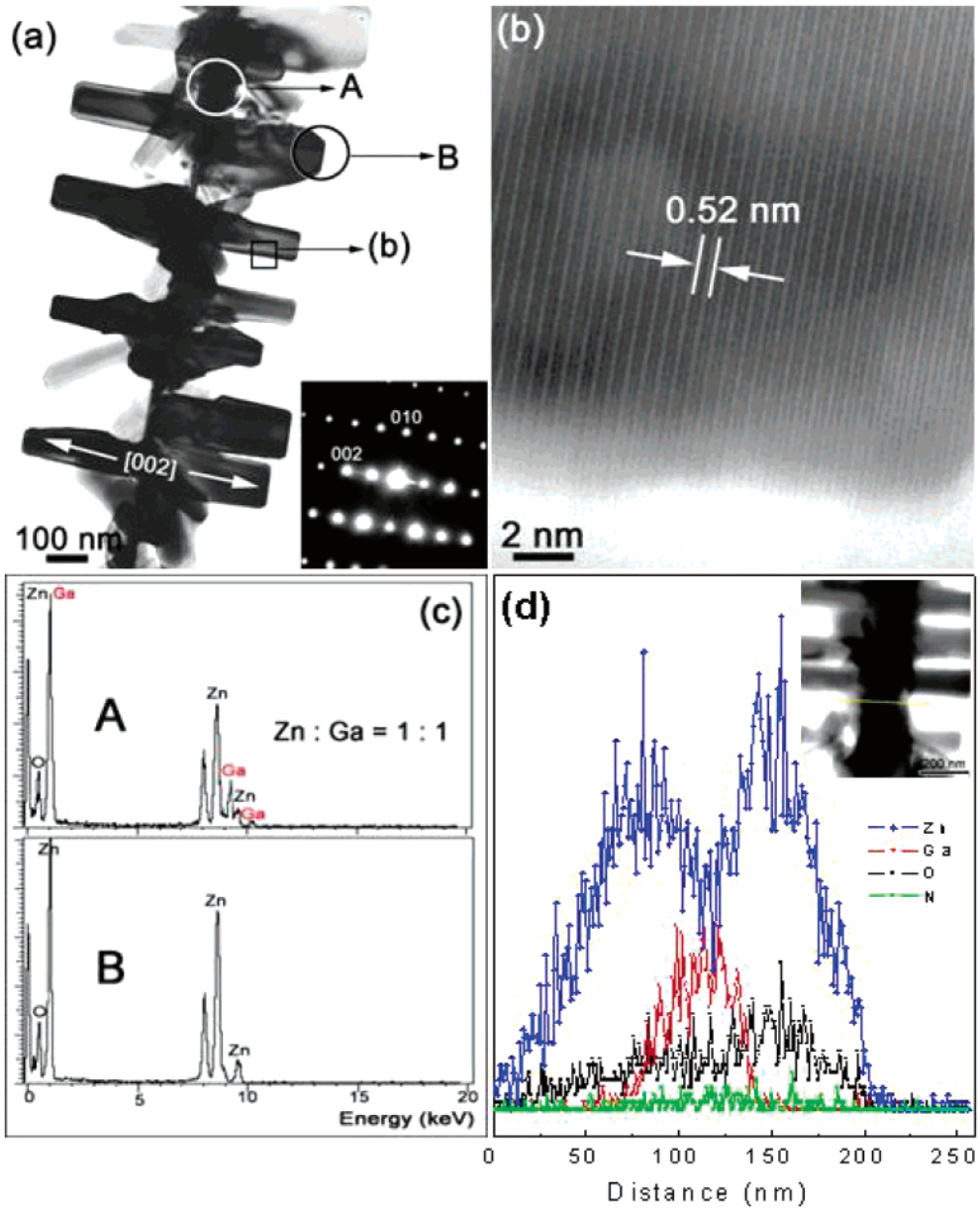

Figure 2. (a) TEM image showing a general morphology of the GaN−ZnO heterostructures that the ZnO nanorods align perpendicularly on the surface of the GaN nanorod. SAED pattern of the ZnO nanorods reveals the [002] growth direction (inset). (b) Atomic-resolved image for the ZnO nanorod, showing that the distance between neighboring (001) planes is about 5.2 Å. (c) EDX of the core part (marked by the arrow "A" in (a)) shows the Zn and Ga components with 1:1 atomic ratio. The side nanorods (marked by the arrow "B" in (a)) consist of only ZnO. (d) EDX line-scan profile of the GaN−ZnO nanostructure whose TEM image is shown in the inset.

the XRD peaks can be powerful supporting data for the uniform growth direction of the nanostructures.

Figure 4a displays the Raman scattering spectrum of SiC−C−ZnO nanostructures. The first-order phonon frequencies of E_2 and E_1(LO) of wurtzite ZnO were reported to be 438 and 590 cm^{-1}, respectively.[27] It is known that the E_1(LO) mode is associated with oxygen deficiency. The spectrum shows the peaks at 438 and 570 cm^{-1}, corresponding to the E_2 and E_1(LO) modes of ZnO. For the peak assignment, the Raman spectrum has been measured for the SiC−C−ZnO nanostructure sample in which the ZnO nanorods were grown for 30 min. Only the tiny E_1(LO) mode peak appears. The peak at 1130 cm^{-1} becomes significant as the intensity of the first-order ZnO peak increases. Therefore, this band can be assigned to the overtone band of the E_1(LO) mode. The spectrums show two strong bands at 1590 and 1354 cm^{-1}, which can be assigned to the G and D bands of CNTs, respectively. A series of small peaks in the range 650−1050 cm^{-1} corresponds to the TO and LO modes of β-SiC. These peaks originate from the SiC−C coaxial nanocables.[27] The intensity of the E_1(LO) mode relative to the E_2 mode is more significant when compared to that of pure ZnO nanorods.[28] The present nanostructures would possess a larger surface area of ZnO nanorods and more interfaces due to the higher density. The oxygen deficiency at those places can play a role in increasing the intensity of the E_1(LO) mode.

Figure 4b shows the Raman scattering spectrum of GaN−ZnO nanostructures. The peaks at 438 and 575 cm^{-1} can be assigned to the E_2 and E_1(LO) modes of ZnO, respectively. The E_2(high) mode of wurtzite GaN crystal appeared at 570 cm^{-1} for the GaN nanowires.[29] Because the E_2(high) mode of GaN overlaps with the E_1(LO) mode of ZnO, the intensity of the ZnO E_1(LO) mode relative to the E_2 mode is more significant when compared to that of the SiC−C−ZnO nanostructures. The peak at 710 cm^{-1} is assigned to the A_1(LO) mode of wurtzite

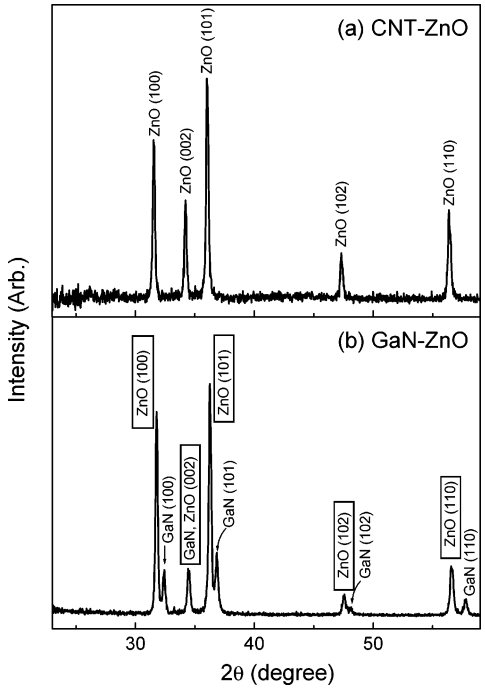

Figure 3. XRD pattern taken from (a) CNT−ZnO and (b) GaN−ZnO heterostructures.

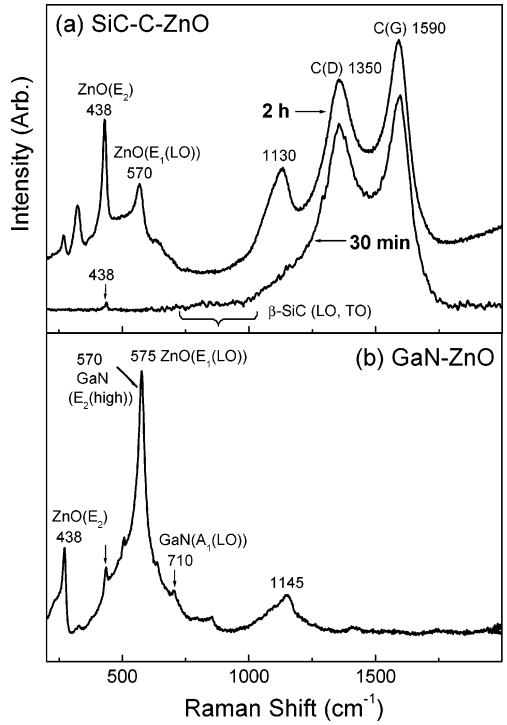

Figure 4. Raman spectrum of (a) SiC−C−ZnO heterostructures grown for 30 min and 2 h and (b) GaN−ZnO heterostructures grown for 2 h. The excitation laser is a 514.5 nm argon ion laser.

GaN crystal. The peak at 1145 cm^{-1} can be an overlapped overtone of the ZnO E_1(LO) and GaN E_2(high) modes.

(3) Growth Mechanism of ZnO Nanorods. We monitored how the deposition of ZnO nanorods takes place on the 1D nanostructures as a function of time. Figure 5a shows a side view of the SiC nanowires grown on the Si substrate. The length is about 300 μm. A magnified image shows that the average diameter is about 50 nm (inset). During 2 h, the deposition of ZnO nanorods covers about two-thirds of the SiC nanowires from the top (Figure 5b). A magnified image for the top part as

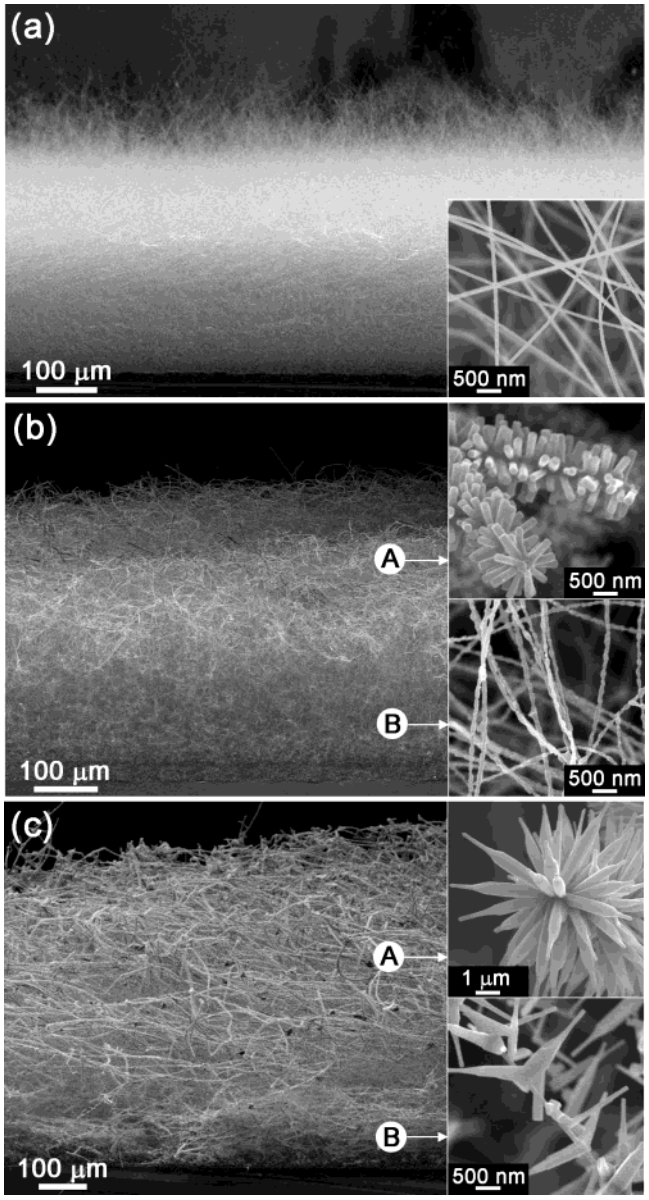

Figure 5. SEM micrographs showing the growth of ZnO nanorods on the SiC nanowires as a function of time: (a) 0 h, (b) 2 h, and (c) 4 h.

indicated by "A" shows that the diameter and length of ZnO nanorods are 100 and 500 nm, respectively. The diameter of the heterostructures is about 1 μm. The lower part (indicated by "B") shows the SiC nanowires coated with the ZnO nanocrystals. The ZnO nanorods deposit over all of the SiC nanowires for 4 h (Figure 5c). The magnified image for the top part indicated by "A" shows that the diameter of the heterostructures increases to 5 μm, due to the 3 μm-long ZnO nanorods. The ZnO nanorods become thicker with a diameter of 300 nm. The initially grown ZnO nanorods remain as a sharp tip having a diameter of 100 nm. In the lower parts indicated by "B", the ZnO nanorods with a length of 1.5 μm deposit on the SiC nanowires.

The time-dependent SEM images of other heterostructures also consistently show that, as the deposition time increases, the length of the ZnO nanorods and the density on individual 1D nanostructures increases with time. The ZnO nanorods frequently show a needle shape because of the increase of diameter during the growth. The progressive growth of ZnO nanorods from the top to the bottom region indicates that the

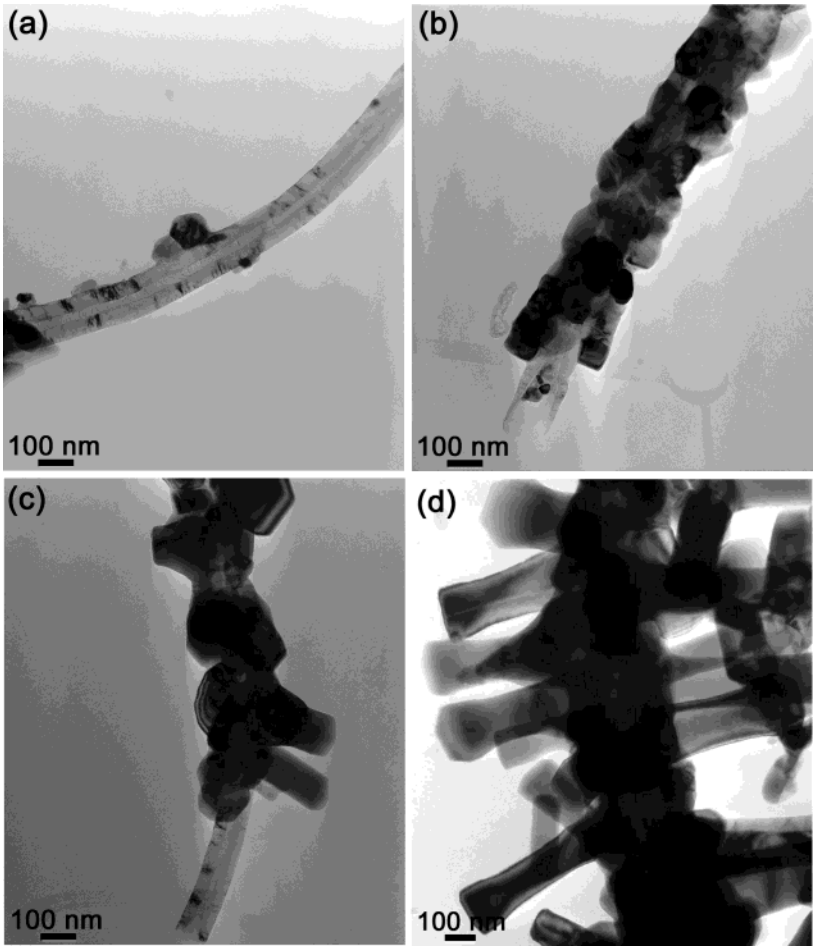

Figure 6. TEM images revealing the general morphology of the CNT−ZnO heterostructures. (a) The nanoparticles start depositing on the CNT; (b) the deposition of the nanoparticles takes place on the whole CNT; (c) a few ZnO nanorods are grown out of the nanoparticles; and (d) the aligned ZnO nanorods are fully grown on the CNT.

Zn and O vapors diffuse from the top to the bottom. The growth of ZnO nanorods would occur under the kinetically controlled condition that the higher Zn and O vapor pressure leads to the higher growth rate of ZnO nanorods.

To elucidate the growth mechanism, we analyzed the TEM images of the CNT−ZnO nanostructures. The corresponding SEM images are shown in Figure 1a−c. Figure 6a displays a CNT decorated with a few number of ZnO nanocrystals. The diameter of CNT is about 100 nm. Figure 6b shows the deposition of ZnO nanocrystals occurring on the whole surface of CNT. The thickness of the deposited layers is about 50 nm. The ZnO nanorods start growing perpendicularly on the wall of CNT, with a diameter of 80 nm (Figure 6c). The ZnO nanorods are grown on the full surface of CNT (Figure 6d).

The SEM and TEM images provide detailed features of the growth process of ZnO nanorods. A schematic diagram using the cross-section of nanostructures is displayed in Figure 7. Zn vapor deposits on a 100-nm diameter CNT and forms the liquid droplets at 500 °C because the melting point is 412 °C (step I). The O component supplied from the residual air can dissolve into the liquid droplets. Further deposition makes the outer layers that encapsulate the CNT, producing a nanocable structure whose outer diameter is larger than 200 nm (step II). The continuously supplied Zn and O vapors saturate into the outer layers, followed by the precipitation of the ZnO nanorods. Step III shows how the ZnO nanorods grow from the outer layers. The outer diameter of the nanocables would restrict the diameter of the ZnO nanorods within a nanometer range. The maximum number and diameter of ZnO nanorods surrounding the nanocables depends on the outer diameter of the CNT−ZnO nanocables. The length of the ZnO nanorods increases with time as shown in step IV. It is also possible that the diameter is not uniform as the growth proceeds. If the diameter of the nanocables increases during the growth, the diameter of ZnO nanorods would increase. The ZnO nanorods then exhibit a needle shape, as shown in the case of SiC−ZnO nanostructures (Figure 5c). Overall, the growth mechanism of ZnO nanorods would be a typical vapor−liquid−solid (VLS) mechanism.

In the case of GaN nanowires, the triangle facet of the deposited outer layers leads to the growth of ZnO nanorods as shown in the schematic diagrams. When the length of the triangle face is about 50 nm and the thickness of the outer layers is 25 nm, the diameter of the ZnO nanorods grown on each face can be 100 nm. We suggest that the thickness of the outer layers determines the diameter of the ZnO nanorods. The three-dimensional (3D) schematic diagram of the growth process is displayed for the aligned ZnO nanorods along the facet of the triangular GaN nanowire.

We found that the use of Ga or In enhances the deposition rate of the ZnO nanorods. The Ga metal forms a eutectic melting point with 2.6 at. % Zn metal at 26 °C, and the In metal forms a eutectic melting point with 3.8 at. % Zn metal at 143.5 °C.[30] They can form a liquid alloy at the growth temperature of 500 °C, increasing the vapor pressure of Zn enough to produce the high-density ZnO nanorods. Although no Ga component is

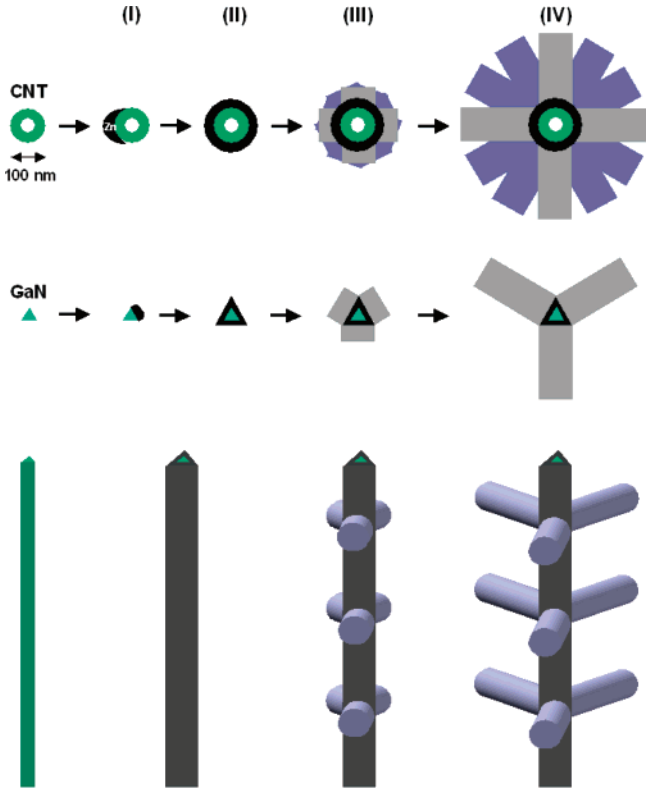

Figure 7. Schematic diagrams using the cross-section of the nanostructures, to show the growth process of ZnO nanorods on the CNT and GaN nanowire; (i) Zn droplets form; (ii) Zn outer layers (marked by black color) encapsulate the CNT (or triangle GaN nanowire); (iii) ZnO nanorods start growing from the outer layers; (iv) aligned ZnO nanorods surround the CNT (or GaN nanowire). 3D diagrams depict the growth process of GaN−ZnO heterostructures.

detected from these ZnO heterostructures by EDX, the Ga (or In) vapor can deposit with the Zn vapor on the surface of 1D nanostructures and facilitates the formation of the liquid droplets by dissolving into them.

As mentioned earlier, the length and density of ZnO nanorods grown for 2 h are dependent on the 1D nanostructures. The shortest length of ZnO nanorods in the case of CNTs could be related to the highest density of CNTs (10^{11} cm^{-2}). We conjecture that the steric hindrance of ZnO nanorods on the neighboring CNTs would lead to a decrease in the density and length of the ZnO nanorods. If the density of the 1D nanostructures were lower, the growth of the ZnO nanorods would be faster. This explains the longer length and higher density of SiC−C nanocables. The triangle cross-section limits the number of ZnO nanorods, yielding a low density.

(4) Optical Properties: PL and CL. The room-temperature (300 K) PL spectra of CNT−ZnO, GaN−ZnO, GaP−ZnO, SiC−ZnO, and SiC−C−ZnO nanostructures are displayed in Figure 8a. The ZnO nanorods were grown for 2 h. For CNT−ZnO, GaP−ZnO, SiC−ZnO, and SiC−C−ZnO nanostructures, the UV emission with a peak at 385 nm (3.22 eV) corresponds to the near band edge (NBE) peak that is responsible for the recombination of free excitons of ZnO.[31] In contrast, the GaN−ZnO nanostructures exhibit a blue-shifted NBE peak at 380 nm (3.26 eV), which is probably related to a contribution of GaN NBE emission that is 359 nm (3.45 eV).[23] There is a broad green emission around 495 nm (2.5 eV) that originates from the recombination of the holes with the electrons occupying the singly ionized oxygen vacancy.[32,33] The SiC−C−ZnO nanostructures exhibit a stronger green emission as compared

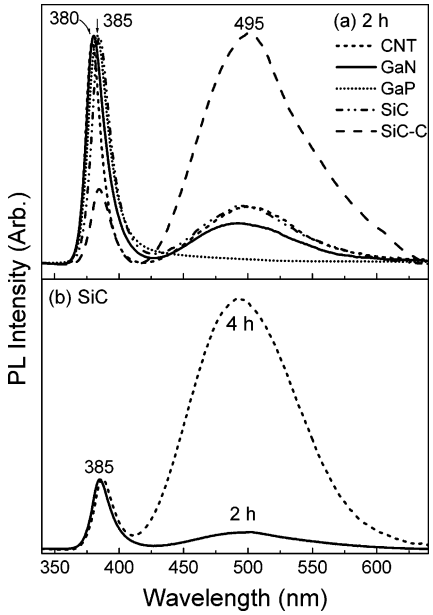

Figure 8. (a) Room-temperature PL spectrum measured from the CNT−ZnO, GaN−ZnO, GaP−ZnO, SiC−ZnO, and SiC−C−ZnO heterostructures grown for 2 h. (b) The PL spectrum of SiC−ZnO heterostructures grown for 2 and 4 h. The excitation wavelength is 325 nm line of a He−Cd laser.

to the others. The intensity of the green emission is even higher than that of the NBE peak.

Figure 8b compares the PL spectrum of SiC−ZnO nanostructures synthesized for 4 h to that of 2 h. The SEM images of the two samples are shown in Figure 5b and c. As the deposition of the ZnO nanorods progresses over all of the SiC nanowires with a higher diameter, length, and density, the intensity of the green emission becomes significant. We also measured the PL spectrum of SiC−C−ZnO nanostructures grown for 30 min, showing that the relative intensity of the green emission band to that of the NBE band decreases by a factor of about 5. Therefore, we conclude that the enhancement of the green emission is strongly correlated with the density of ZnO nanorods on the 1D nanostructures. The relative intensity of the green emission band to the NBE band follows the order SiC−C nanocables > SiC nanowires ≈ CNTs > GaN nanowires > GaP nanowires, which is consistent with the relative density of ZnO nanorods. It can result from the oxygen deficiencies at the increased surface area of ZnO nanorods and more interfaces with the core part.

Figure 9a shows the CL spectrum of GaN−ZnO, SiC−ZnO, and SiC−C−ZnO nanostructures measured at room temperature. The NBE peak of SiC−ZnO and SiC−C−ZnO appears at 388 nm, while that of GaN−ZnO is blue-shifted to 383 nm. The relative intensity of the green emission band to the NBE band follows the order SiC−C > SiC > GaN. These results are consistent with those of PL. The CL image of the SiC−C−ZnO nanostructures is displayed in Figure 9b, revealing the stronger emission from the core part, which can be due to a significant green emission at the interface.

4. Conclusions

We synthesized the ZnO heteronanostructures during which the high-density ZnO nanorods deposit on pregrown CNTs, GaN nanowires, GaP nanowires, SiC nanowires, and SiC−C coaxial nanocables whose syntheses were reported previously. The deposition of ZnO nanorods on these 1D nanostructures was produced via thermal CVD of Zn at 500 °C. Ga or In was used

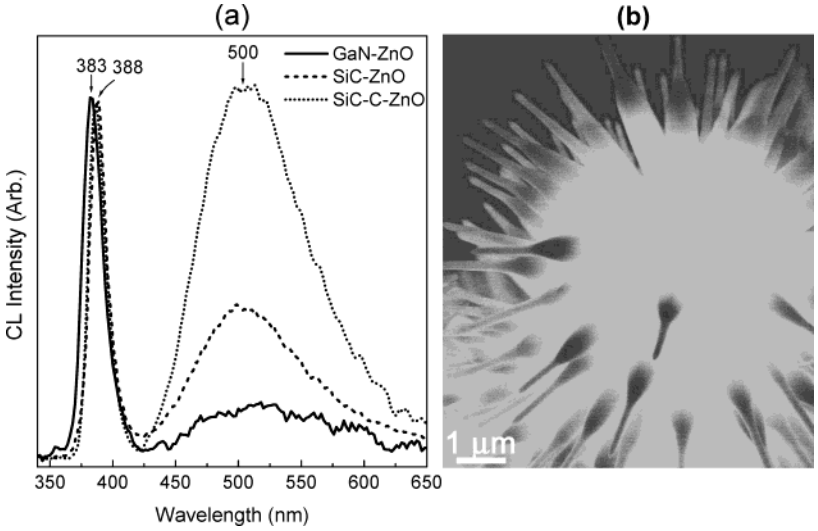

Figure 9. Room-temperature CL spectrum of (a) GaN−ZnO, SiC−ZnO, and SiC−C−ZnO heterostructures grown for 2 h and (b) CL image of a SiC−C−ZnO heterostructure.

as catalyst. The structure, growth mechanism, and optical properties of the heterostructures were investigated using SEM, TEM, EDX, XRD, Raman spectroscopy, PL, and CL. The results are summarized as follows.

(1) The ZnO nanorods align vertically on the wall of these 1D nanostructures. The growth direction of the ZnO nanorods is uniformly [001]. The symmetric alignment of the ZnO nanorods was observed for the GaN−ZnO nanostructures. The diameter of the ZnO nanorods is in the range 80−150 nm, and the length is up to 3 μm.

(2) The growth of the ZnO nanorods was monitored as a function of time, revealing that the deposition of the ZnO nanorods starts from the top part of 1D nanostructures. As the deposition time increases, the length and density can increase. The diameter frequently increases with the time. We suggest that the growth of the ZnO nanorods would follow a VLS growth mechanism. Zn vapor deposits on the 1D nanostructures and forms the nanocable structure that the outer layers encapsulate in the 1D nanostructure. The ZnO nanorods grow out from the outer layers of the nanocables, and the diameter is determined by the diameter of the nanocables. The triangle facet of the outer layers leads the ZnO nanorods to align in a row on the wall of the GaN nanowires.

(3) The heterostructures exhibit intense PL in the UV region with a peak of 385 nm, corresponding to the NBE peak of ZnO nanorods. For GaN−ZnO nanostructures, the NBE peak shows a blue-shift to 380 nm, because of the emission of GaN nanowires. The CL shows a good consistency with the PL. The relative intensity of the green emission band to that of the NBE band increases with the density of ZnO nanorods. This can be due to the higher oxygen vacancies at the increased surface area and more interfaces. We recommend that these heterostructures can be promising candidates for the light emitting diode devices, with respect to the high-density ZnO nanorods forming the 3D hierarchical structures.

Acknowledgment. The Korea Science and Engineering Foundation (Project No.: R14-2003-033-01003-0) and Korea Research Foundation (Project No.: 2003-015-C00265) supported the present work. SEM and X-ray diffraction analyses were performed at the Korea Basic Research Institute in Seoul.

References and Notes

(1) Iijima, S. *Nature* **1991**, *354*, 56.

(2) (a) Duan, X.; Huang, Y.; Cui, Y.; Wang, J.; Lieber, C. M. *Nature* **2001**, *409*, 66. (b) Gudiksen, M. S.; Duan, X.; Cui, Y.; Lieber, C. M. *Science* **2001**, *293*, 1455. (c) Huang, Y.; Duan, X.; Cui, Y.; Lauhon, L. J.; Kim, K.-H.; Lieber, C. M. *Science* **2001**, *294*, 1313. (d) Tseng, G. Y.; Ellenbogen, J. C. *Science* **2001**, *294*, 1293. (e) Duan, X.; Huang, Y.; Agarwal, R.; Lieber, C. M. *Nature* **2003**, *421*, 241. (f) Melosh, N. A.; Boukai, A.; Diana, F.; Gerardot, B.; Badolato, A.; Petroff, P. M.; Heath, J. R. *Science* **2003**, *300*, 112. (g) Xia, Y.; Yang, P.; Sun, Y.; Wu, Y.; Mayers, B.; Gates, B.; Yin, Y.; Kim, F.; Yan, H. *Adv. Mater.* **2003**, *15*, 353.

(3) (a) Hu, J.; Ouyang, M.; Yang, P.; Lieber, C. M. *Nature* **1999**, *399*, 48. (b) Zhang, Y.; Ichihashi, T.; Landree, E.; Nihey, F.; Iijima, S. *Science* **1999**, *285*, 1719. (c) Luo, J.; Zhang, L.; Zhu, J. *Adv. Mater.* **2003**, *15*, 579.

(4) (a) Nicewarner-Pena, S. R.; Freeman, R. G.; Reiss, B. D.; He, L.; Pena, D. J.; Walton, I. D.; Cromer, R.; Keating, C. D.; Natan, M. J. *Science* **2001**, *294*, 137. (b) Gudiksen, M. S.; Lauhon, L. J.; Wang, J.; Smith, D. C.; Lieber, C. M. *Nature* **2002**, *415*, 617. (c) Wu, Y.; Fan, R.; Yang, P. *Nano Lett.* **2002**, *2*, 83.

(5) (a) Zhang, Y.; Suenaga, K.; Colliex, C.; Iijima, S. *Science* **1998**, *281*, 973. (b) Lauhon, L. J.; Gudiksen, M. S.; Wang, D.; Lieber, C. M. *Nature* **2002**, *420*, 57. (c) Han, W.; Zettl, A. *Adv. Mater.* **2002**, *14*, 1560. (d) Hu, J.-Q.; Meng, X.-M.; Jiang, Y.; Lee, C.-S.; Lee, S.-T. *Adv. Mater.* **2003**, *15*, 70. (e) Li, Y.; Bando, Y.; Golberg, D. *Adv. Mater.* **2004**, *16*, 93.

(6) (a) He, R.; Law, M.; Fan, R.; Kim, F.; Yang, P. *Nano Lett.* **2002**, *2*, 1109. (b) Hu, J.; Bando, Y.; Liu, Z.; Sekiguchi, T.; Golberg, D.; Zhan, J. *J. Am. Chem. Soc.* **2003**, *125*, 11306.

(7) Cao, H.; Xu, J. Y.; Zhang, D. Z.; Chang, S.-H.; Ho, S. T.; Seelig, E. W.; Liu, X.; Chang, R. P. H. *Phys. Rev. Lett.* **2000**, *84*, 5584.

(8) Dong, L. F.; Cui, Z. L.; Zhang, Z. K. *Nanostruct. Mater.* **1997**, *8*, 815.

(9) (a) Huang, M. H.; Wu, Y.; Feick, H.; Tran, N.; Weber, E.; Yang, P. *Adv. Mater.* **2001**, *13*, 113. (b) Huang, M. H.; Mao, S.; Feick, H.; Yan, H.; Wu, Y.; Kind, H.; Weber, E.; Russo, R.; Yang, P. *Science* **2001**, *292*, 1897. (c) Wu, J.-J.; Liu, S.-C. *Adv. Mater.* **2002**, *14*, 215. (d) Johnson, J. C.; Yan, H.; Schaller, R. D.; Petersen, P. B.; Yang, P.; Saykally, R. J. *Nano Lett.* **2002**, *2*, 279. (e) Guo, L.; Ji, Y. L.; Xu, H.; Simon, P.; Wu, Z. *J. Am. Chem. Soc.* **2002**, *124*, 14864. (f) Pacholski, C.; Kornowski, A.; Weller, H. *Angew. Chem., Int. Ed.* **2002**, *41*, 1188. (g) Liu, B.; Zeng, H. C. *J. Am. Chem. Soc.* **2003**, *125*, 4430. (h) Vayssieres, L. *Adv. Mater.* **2003**, *15*, 464. (i) Liu, C.; Zapien, J. A.; Yao, Y.; Meng, X.; Lee, C. S.; Fan, S.; Lifshitz, Y.; Lee, S. T. *Adv. Mater.* **2003**, *16*, 838. (j) Ng, H. T.; Li, J.; Smith, M. K.; Nguyen, P.; Cassell, A.; Han, J.; Meyyappan, M. *Science* **2003**, *300*, 1249. (k) Zhao, Q. X.; Willander, M.; Morjan, R. E.; Hu, Q.-H.; Campbell, E. E. B. *Appl. Phys. Lett.* **2003**, *83*, 165. (l) Johnson, J. C.; Yan, H.; Yang, P.; Saykally, R. J. *J. Phys. Chem. B* **2003**, *107*, 8816. (m) Lyu, S. C.; Zhang, Y.; Lee, C. J.; Ruh, H.; Lee, H. J. *Chem. Mater.* **2003**, *15*, 3294. (n) Greene, L. E.; Law, M.; Goldberger, J.; Kim, F.; Johnson, J. C.; Zhang, Y.; Saykally, R. J.; Yang, P. *Angew. Chem., Int. Ed.* **2003**, *42*, 3031. (o) Zhong, J.; Muthukumar, S.; Chen, Y.; Lu, Y.; Ng, H. M.; Jiang, W.; Garfunkel, E. L. *Appl. Phys. Lett.* **2003**, *83*, 3401. (p) Monge, M.; Kahn, M. L.; Maisonnat, A.; Chaudret, B. *Angew. Chem., Int. Ed.* **2003**, *42*, 5321. (q) Chang, Y. Q.;

Wang, D. B.; Luo, X. H.; Xu, X. Y.; Chen, X. H.; Li, L.; Chen, C. P.; Wang, R. M.; Xu, J.; Yu, D. P. *Appl. Phys. Lett.* **2003**, *83*, 4020. (r) Choy, J.-H.; Jang, E.-S.; Won, J.-H.; Chung, J.-H.; Jang, D.-J.; Kim, Y.-W. *Adv. Mater*. **2003**, *15*, 1911. (s) Zhang, B. P.; Binh, N. T.; Segawa, Y.; Kashiwaba, Y.; Haga, K. *Appl. Phys. Lett.* **2004**, *84*, 586.

(10) (a) Wu, J.-J.; Liu, S.-C.; Wu, C.-T.; Chen, K.-H.; Chen, L.-C. *Appl. Phys. Lett*. **2002**, *81*, 1312. (b) Hu, J. Q.; Li, Q.; Meng, X. M.; Lee, C. S.; Lee, S. T. *Chem. Mater*. **2003**, *15*, 305. (c) Zhang, X.-H.; Xie, S.-Y.; Jiang, Z.-Y.; Zhang, X.; Tian, Z.-Q.; Xie, Z.-X.; Huang, R.-B.; Zheng, L.-S. *J. Phys. Chem. B* **2003**, *107*, 10114. (d) Xing, Y. J.; Xi, Z. H.; Xue, Z. Q.; Zhang, X. D.; Song, J. H.; Wang, R. M.; Xu, J.; Song, Y.; Zhang, S. L.; Yu, D. P. *Appl. Phys. Lett.* **2003**, *83*, 1689. (e) Wang, R. M.; Xing, Y. J.; Xu, J.; Yu, D. P. *New J. Phys*. **2003**, *5*, 115. (f) Kim, H.; Sigmund, W. M. *J. Mater. Res*. **2002**, *18*, 2845. (g) Kong, X.; Sun, X.; Li, X.; Li, Y. *Mater. Chem. Phys*. **2003**, *82*, 997. (h) Kong, X. Y.; Ding, Y.; Wang, Z. L. *J. Phys. Chem. B* **2004**, *108*, 570.

(11) (a) Pan, Z. W.; Dai, Z. R.; Wang, Z. L. *Science* **2001**, *291*, 1947. (b) Li, Y. B.; Bando, Y.; Sato, T.; Kurashima, K. *Appl. Phys. Lett*. **2002**, *81*, 144. (c) Dai, Z. R.; Pan, Z. W.; Wang, Z. L. *Adv. Funct. Mater*. **2003**, *13*, 9. (d) Bai, X.; Wang, E. G.; Gao, P.; Wang, Z. L. *Nano Lett.* **2003**, *3*, 1147. (e) Bai, X. D.; Gao, P. X.; Wang, Z. L.; Wang, E. G. *Appl. Phys. Lett*. **2003**, *82*, 4806. (f) Yan, Y.; Liu, P.; Wen, J. G.; To, B.; Al-Jassim, M. M. *J. Phys. Chem. B* **2003**, *107*, 9701. (g) Yan, H.; Johnson, J.; Law, M.; He, R.; Knutsen, K.; McKinney, J. R.; Pham, J.; Saykally, R.; Yang, P. *Adv. Mater*. **2003**, *15*, 1907. (h) Kong, X. Y.; Wang, Z. L. *Nano Lett*. **2003**, *3*, 1625. (i) Hughes, W. L.; Wang, Z. L. *Appl. Phys. Lett.* **2003**, *82*, 2886. (j) Mao, S. X.; Zhao, M. H.; Wang, Z. L. *Appl. Phys. Lett*. **2003**, *83*, 993. (k) Arnold, M. S.; Avouris, P.; Pan, Z. W.; Wang, Z. L. *J. Phys. Chem. B* **2003**, *107*, 659. (l) Li, Y.; You, L.; Duan, R.; Shi, P.; Qin, G. *Solid State Commun*. **2004**, *129*, 233. (m) Ronning, C.; Gao, P. X.; Ding, Y.; Wang, Z. L.; Schwen, D. *Appl. Phys. Lett.* **2004**, *84*, 783.

(12) (a) Dai, Y.; Zhang, Y.; Li, Q. K.; Nan, C. W. *Chem. Phys. Lett*. **2002**, *358*, 83. (b) Yan, H.; He, R.; Pham, J.; Yang, P. *Adv. Mater*. **2003**, *15*, 402. (c) Dai, Y.; Zhang, Y.; Wang, Z. L. *Solid State Commun*. **2003**, *126*, 629. (d) Roy, V. A. L.; Djurisic, A. B.; Chan, W. K.; Gao, J.; Lui, H. F.; Surya, C. *Appl. Phys. Lett*. **2003**, *83*, 141. (e) Zhang, Y.; Jia, H.; Luo, X.; Chen, X.; Yu, D.; Wang, R. *J. Phys. Chem. B* **2003**, *107*, 8289. (f) Wan, Q.; Yu, K.; Wang, T. H.; Lin, C. L. *Appl. Phys. Lett.* **2003**, *83*, 2253. (g) Roy, V. A. L.; Djurisic, A. B.; Liu, H.; Zhang, X. X.; Leung, Y. H.; Xie, M. H.; Gao, J.; Lui, H. F.; Surya, C. *Appl. Phys. Lett*. **2004**, *84*, 756.

(13) (a) Park, W. I.; Yi, G.-C.; Kim, M.; Pennycook, S. J. *Adv. Mater*. **2002**, *14*, 1841. (b) Zhu, Y. W.; Zhang, H. Z.; Sun, X. C.; Feng, S. Q.; Xu, J.; Zhao, Q.; Xiang, B.; Wang, R. M.; Yu, D. P. *Appl. Phys. Lett*. **2003**, *83*, 144. (c) Tseng, Y.-K.; Huang, C.-J.; Cheng, H.-M.; Lin, I.-N.; Liu, K.-S.; Chen, I.-C. *Adv. Funct. Mater*. **2003**, *13*, 811.

(14) Xu, C. X.; Sun, X. W. *Appl. Phys. Lett*. **2003**, *83*, 3806.

(15) (a) Tian, Z. R.; Voigt, J. A.; Liu, J.; Mckenzie, B.; Mcdermott, M. J. *J. Am. Chem. Soc.* **2002**, *124*, 12954. (b) Hu, P.; Liu, Y.; Wang, X.; Fu, L.; Zhu, D. *Chem. Commun*. **2003**, *11*, 1304.

(16) (a) Yan, H.; He, R.; Johnson, J.; Law, M.; Saykally, R. J.; Yang, P. *J. Am. Chem. Soc.* **2003**, *125*, 4728. (b) Wang, Z. L.; Kong, X. Y.; Zuo, J. M. *Phys. Rev. Lett*. **2003**, *91*, 185502.

(17) (a) Yu, S.-H.; Yang, J.; Qian, Y.-T.; Yoshimura, M. *Chem. Phys. Lett*. **2002**, *361*, 362. (b) Hu, J. Q.; Bando, Y.; Zhan, J. H.; Li, Y. B.; Sekiguchi, T. *Appl. Phys. Lett*. **2003**, *83*, 4414. (c) Park, J.-H.; Choi, H.-J.; Choi, Y.-J.; Sohn, S.-H.; Park, J.-G. *J. Mater. Chem*. **2003**, *14*, 35.

(18) (a) Gao, P.; Wang, Z. L. *J. Phys. Chem. B* **2002**, *106*, 12653. (b) Lao, J. Y.; Huang, J. Y.; Wang, D. Z.; Ren, Z. F. *Nano Lett*. **2003**, *3*, 235. (c) Tian, Z. R.; Voigt, J. A.; Liu, J.; Mckenzie, B.; Mcdermott, M. J.; Rodriguez, M. A.; Konishi, H.; Xu, H. *Nat. Mater*. **2003**, *2*, 821. (d) Hu, P.-A.; Liu, Y.-Q.; Fu, L.; Wang, X.-B.; Zhu, D.-B. *Appl. Phys. A* **2004**, *78*, 15.

(19) (a) Wang, X.; Gao, P.; Li, J.; Summers, C. J.; Wang, Z. L. *Adv. Mater*. **2002**, *14*, 1732. (b) Zhou, H.; Alves, H.; Hofmann, D. M.; Kriegseis, W.; Meyer, B. K.; Kaczmarczyk, G.; Hoffmann, A. *Appl. Phys. Lett*. **2002**, *80*, 210. (c) Hu, J.; Bando, Y.; Liu, Z. *Adv. Mater*. **2003**, *15*, 1000. (d) Min, B.; Lee, J. S.; Hwang, J. W.; Keem, K. H.; Kang, M. I.; Cho, K.; Sung, M. Y.; Kim, S.; Lee, M. S.; Park, S. O.; Moon, J. T. *J. Cryst. Growth* **2003**, *252*, 565. (e) Dai, L.; Chen, X. L.; Zhang, X.; Zhou, T.; Hu, B. *Appl. Phys. A* **2004**, *78*, 557. (f) Ding, Y.; Kong, X. Y.; Wang, Z. L. *J. Appl. Phys*. **2004**, *95*, 306.

(20) (a) Kim, H.; Sigmund, W. *Appl. Phys. Lett*. **2002**, *81*, 2085. (b) Lao, J. Y.; Wen, J. G.; Ren, Z. F. *Nano Lett*. **2002**, *2*, 1287.

(21) (a) Park, W. I.; Yi, G.-C.; Kim, M.; Pennycook, S. J. *Adv. Mater*. **2003**, *15*, 526. (b) Jung, S. W.; Park, W. I.; Yi, G.-C.; Kim, M. *Adv. Mater*. **2003**, *15*, 1358.

(22) Lee, Y. T.; Park, J.; Choi, Y. S.; Ryu, H.; Lee, H. J. *J. Phys. Chem. B* **2002**, *106*, 7614.

(23) Bae, S. Y.; Seo, H. W.; Park, J.; Yang, H.; Kim, H.; Kim, S. *Appl. Phys. Lett*. **2003**, *82*, 4564.

(24) Seo, H. W.; Bae, S. Y.; Park, J.; Yang, H.; Kim, S. *Chem. Commun.* **2002**, 2564.

(25) Kim, H. Y.; Park, J.; Yang, H. *Chem. Commun.* **2003**, *20*, 256.

(26) Kim, H. Y.; Bae, S. Y.; Kim, N. S.; Park, J. *Chem. Commun*. **2003**, *20*, 2634.

(27) Exarhos, G. J.; Sharma, S. K. *Thin Solid Films* **1995**, *270*, 27.

(28) Seo, H. W.; Bae, S. Y.; Park, J. *J. Phys. Chem. B*, in press.

(29) Azuhata, T.; Sota, T.; Suzuki, K.; Nakamura, S. *J. Phys.: Condens. Matter* **1995**, *7*, L129.

(30) *Binary Alloy Phase Diagrams*; Massalski, T. B., Murray, J. L., Bennett, L. H., Baker, H., Eds.; American Society for Metals: Metals Park, 1986.

(31) Kong, Y. C.; Yu, D. P.; Zhang, B.; Fang, W.; Feng, S. Q. *Appl. Phys. Lett*. **2001**, *78*, 407.

(32) Vanheusden, K.; Warren, W. L.; Seager, C. H.; Tallant, D. R.; Voigt, J. A.; Gnade, B. E. *J. Appl. Phys*. **1996**, *79*, 7983.

(33) Wu, X. L.; Siu, G. G.; Fu, C. L.; Ong, H. C. *Appl. Phys. Lett.* **2001**, *78*, 2285.